Defect-induced spin deterioration of $La_{0.64}Sr_{0.36}MnO_3$: *Ab initio* study

Kunpeng Wang, Yuchen Ma, and Klaus Betzler*
Fachbereich Physik, Universität Osnabrück, D-49069 Osnabrück, Germany
(Received 17 July 2007; revised manuscript received 8 August 2007; published 26 October 2007)

We present an *ab initio* study of the effect of various point defects with different concentrations on the magnetic properties of $La_{0.64}Sr_{0.36}MnO_3$ (LSMO). We find that the 100% spin polarization is destroyed by oxygen vacancies with a concentration of 11.1% and by O substituting for La (La_v+O_i pair) with a concentration of 12.5%. Interstitial oxygen defects make no contribution to the spin deterioration of LSMO at the Fermi level despite the theoretical half-metallic gap is decreased. When the La/Sr vacancy concentration increases up to 25.0%, the majority spin at the Fermi level is decreased dramatically. The results elucidate the underlying mechanism for the deterioration of the spin polarization of LSMO.

DOI: 10.1103/PhysRevB.76.144431 PACS number(s): 72.25.−b, 71.55.−i, 75.47.Lx

A strong revival of research for the doped perovskite manganites, $(La,A)MnO_3$ $(A=Sr,Ca,Pb,Ba)$, occurred around 1995 (for reviews see Ref. 1), because of their potential candidates for the future high performance spintronic devices.[2] In particular, the optimally doped $La_{2/3}Sr_{1/3}MnO_3$ (LSMO) exhibits extremely large negative magnetoresistivities and 100% spin polarization of the charge carriers at the Fermi level E_F,[3–5] which make it very appealing for spin injection in devices for spintronics.[6,7] For example, LSMO/$SrTiO_3$ (STO)/LSMO magnetic tunneling junctions display very high values of the tunneling magnetoresistance (TMR) at 4.2 K (1800%).[4] More recently, the spin information of LSMO has been successfully transformated into large electrical signals (65 mV) at 5 K by a molecular spintronic device.[8] Despite the encouraging results, the TMR, for example, in the junctions LSMO/STO/LSMO, has been much smaller than that expected from the half-metallic nature of LSMO. The possible origin of the decreased magneto resistance is suggested to be the deterioration of the interfacial spin state.[9] However, we suggest that the point defects in LSMO may also play an important role. Furthermore, understanding the point defects in LSMO itself is also a subject of great interest and importance in improving device performance and material quality. Despite experimental and theoretical efforts have predominantly focused on understanding the role of oxygen vacancy,[10,11] there is still a controversy over the effect of defects on the magnetic properties of LSMO.

In this paper, we present an overall *ab initio* study of various point defects with different concentrations in LSMO: (1) O vacancies of 2.08% ($O_{v2.08}$), 4.16% ($O'_{v4.16}$ and $O''_{v4.16}$ located at different positions), 8.33% ($O_{v8.33}$), and 11.1% ($O_{v11.1}$); (2) interstitial O of 2.08% ($O_{i2.08}$), 4.16% ($O_{i4.16}$), and 8.33% ($O_{i8.33}$); (3) O Frenkel pair or O_v+O_i; (4) La/Sr vacancies of 6.25% ($La_{v6.25}$), 12.5% ($La_{v12.5}$), 12.5% ($Sr_{v12.5}$), and 25.0% ($La/Sr_{v25.0}$); and (5) O substituting for La or La_v+O_i pair of 6.25% ($O_{La6.25}$), 12.5% ($O_{La12.5}$), and 25.0% ($O_{La25.0}$). The calculations elucidate the key role of various point defects in the magnetic properties of LSMO. We find that the 100% spin polarization is destroyed by oxygen vacancies with a concentration of 11.1% and by O substituting for La with a concentration of 12.5%. Interstitial oxygen defects make no contribution to the spin deterioration of LSMO.

The *ab initio* calculations we performed are based on density-functional theory with the SIESTA implementation.[12] Geometry optimization and energy calculations were carried out with the spin-polarized generalized-gradient approximation (GGA) using the Perdew-Burke-Ernzerhof[13] for electron exchange and correlation. The pseudopotentials were generated using the following reference configurations: $5s^25p^65d^04f^0$ for La, $3s^23p^63d^54f^0$ for Mn, $4s^24p^64d^04f^0$ for Sr, and $2s^22p^43d^04f^0$ for O. The core radii for the *s*, *p*, *d*, and *f* states were $1.85a_0$, $2.20a_0$, $3.10a_0$, and $1.40a_0$ for La, $1.40a_0$, $1.90a_0$, $1.50a_0$, and $1.90a_0$ for Mn, $1.50a_0$, $1.50a_0$, $2.00a_0$, and $2.0a_0$ for Sr, and $1.15a_0$, $1.15a_0$, $1.15a_0$, and $1.50a_0$ for O. The basis set consists of strictly localized atomic orbitals at the double-ζ polarized level,[14] and the semicore states are treated at the single-ζ level. In general, local-density approximation including Coulomb correlation effect (LDA+*U*) approach[15] is thought to be necessary for the study of electronic and magnetic properties of transition-metal oxides. However, recent works suggest that the bare GGA offers a good description of both the structure[8,16,17] and magnetic properties[11,18] of manganites, which allows obtaining full relaxed geometries within bare GGA for defect structures. Based on the experimental $La_{0.64}Sr_{0.36}MnO_3$ structure ($\bar{R}3C$ space group with $Z=6$, pseudocubic lattice parameter $a_{expt}=3.89$ Å, ICSD-95568),[19] we construct a repeated supercell which contains 40 atoms (8 LSMO f.u.) with lattice vectors $a=5.503$ Å, $b=9.532$ Å, $c=9.461$ Å, $\alpha=109.623°$, and $\beta=\gamma=90°$ to simulate an isolated point defect. Three La atoms in the supercell are substituted by Sr in order to simulate the 0.36 Sr doping. So the actual Sr doping content (3/8=0.375) is 0.015 higher than the experimental value of 0.36. The doping configurations have 17 types. We performed the total-energy calculations for all the 17 configurations without atom relaxation and take the lowest energy structure as the initial configuration, which is then fully relaxed including all atoms and lattice constants and was used as the initial structure for the corresponding defect system. The total energies were well converged with a cutoff of 200 Ry. Integrations over the Brillouin zone were done using the Monkhorst-Pack scheme with 48 *k* points in the relevant irreducible wedge. The relaxed lattice vectors are $a=5.566$ Å, $b=9.641$ Å, $c=9.525$ Å, $\alpha=109.754°$, and $\beta=\gamma=90°$, respectively (an overestimation of 1%), and the total

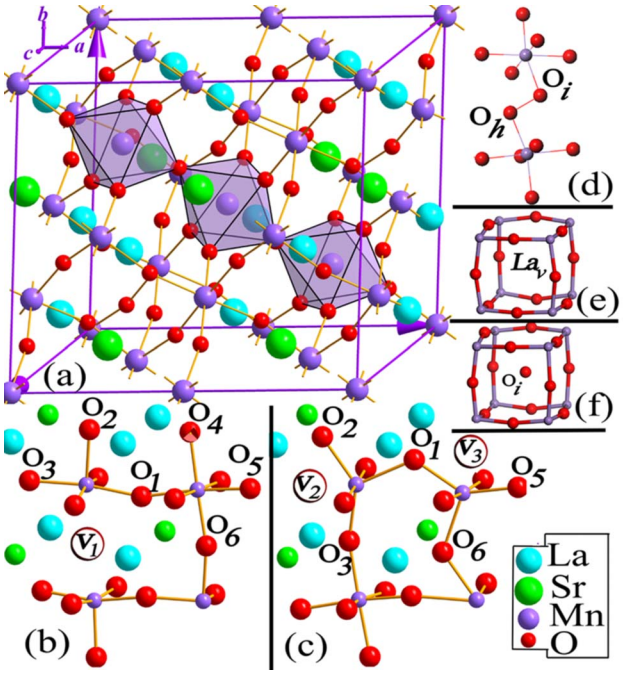

FIG. 1. (Color online) (a) The optimized crystal structure (the supercell contains 80 atoms) for the defect-free LSMO, and (b) the change of the relaxed atomic structure induced by a few representative cases, namely, isolated oxygen vacancy $O_{v4.16}^{\cdot\cdot}$, (c) double O vacancies $O_{v8.33}$, (d) interstitial oxygen $O_{i2.08}$, (e) La vacancy $La_{v6.25}$, and (f) O substituting for La point defect $O_{La12.5}$.

energy gains 0.46 eV. Then, we double the lattice along the *a* direction of the supercell, shown in Fig. 1(a), to simulate defects with lower concentration. For a single O, La, or Sr vacancy, we remove an O, La, or Sr atom from the supercell. For the case of an O Frenkel pair, we remove an O from its regular site in the Mn-O-Mn chain and initially place it in the middle of two La atoms. All results are obtained for the fully relaxed geometries including all atoms and the lattice constants of the supercell with the use of the conjugate gradient techniques. In addition, we also use 15 atoms with 1/3 Sr doping to simulate O vacancies with a concentration of 1/9=11.1%, and the results are in good agreement with those obtained by Picozzi *et al.*[11]

The formation energy for a single vacancy or interstitial can be obtained using the expression $E_F=E^{N\pm1}-E^N\mp\mu$, where $E^{N\pm1}$ is the total energy of the defective supercell, E^N is the energy for the defect-free supercell, and μ is the chemical potential of atoms.[20] Here, we chose for reference states the elements in their standard states,[21] i.e., di-oxygen molecule and La/Sr bulk metal. The calculated formation energies of various point defects are listed in Table I.

Figure 1 shows the optimized crystal structure (the supercell contains 80 atoms) for the defect-free LSMO [Fig. 1(a)], and the change of the relaxed atomic structure induced by a few representative cases, namely, isolated oxygen vacancy $O_{v4.16}^{\cdot\cdot}$ [Fig. 1(b)], double O vacancies $O_{v8.33}$ [Fig. 1(c)], interstitial oxygen $O_{i2.08}$ [Fig. 1(d)], La vacancy $La_{v6.25}$ [Fig. 1(e)], and O substituting for La point defect $O_{La12.5}$ [Fig. 1(f)].

For the isolated oxygen vacancy $O_{v2.08}$, $O_{v4.16}'$, and $O_{v4.16}^{\cdot\cdot}$, the calculated formation energies (at zero temperature and low O pressure) are 6.03, 5.81, and 5.86 eV, respectively, indicating that even in the 40 atom supercells ($O_{v4.16}'$ and $O_{v4.16}^{\cdot\cdot}$), there is a significant vacancy-vacancy interaction on the order of 0.2 eV. As for the optimized atomic structures, there is no significant difference among the isolated $O_{v2.08}$, $O_{v4.16}'$, and $O_{v4.16}^{\cdot\cdot}$ defects. Taking $O_{v4.16}^{\cdot\cdot}$ [Fig. 1(b)] as an example, the neighboring eight O atoms around the oxygen vacancy (V_1) move toward the vacancy and the displacements are in the range of 0.05–0.35 Å, resulting in the decrease of the O-Mn-O bond angles by about 5.11°–12.68°. Conversely, the La/Sr and Mn atoms move away from the vacancy and the maximum displacements are 0.21 for La, 0.09 for Sr, and 0.06 Å for Mn, leading to an increase of the Mn-Mn separation to 4.01 Å from the corresponding value of 3.91 Å in perfect LSMO. However, the removal of O_4, labeled as V_3 in Fig. 1(c), yields a 40° clockwise rotation of the O_1-O_5-O_6 and, however, a nonrigid 38° anticlockwise rotation of O_1-O_2-O_3. The most remarkable feature is that the O_3 atom has anticlockwise rotated about 90° and occupies the site of V_1, resulting in the recovering of the oxygen vacancy V_1 and at the same time leaving behind a new oxygen vacancy V_2. Namely, V_3 yields a migration of V_1 to V_2 site.

For the interstitial oxygen with concentrations of $O_{i2.08}$ and $O_{i4.16}$, the calculated formation energies are 1.36 and 1.14 eV which are higher than the values of KH_2PO_4 (0.6 eV) Ref. 22 and uranium dioxide (−2.9 eV).[20] From Fig. 1(d), we can see that the interstitial oxygen O_i bonds with the host O_h atom creating an extra O_i-O_h bond (1.536 Å), which is larger than the peroxy1 bridge in vitreous silica dioxide (1.49 Å).[23] In other words, the original Mn-O_h-Mn chain is broken and a new Mn-O_h-O_i-Mn chain is formed, leading to an increase of the Mn-Mn separation to 4.31 Å. For O Frenkel pair (O_v+O_i), the O_i comes back to its formal site after fully relaxation, implying that no O Frenkel pairs exist in the LSMO.

For isolated La/Sr vacancies $La_{v6.25}$, $La_{v12.5}$, and $Sr_{v12.5}$, the calculated formation energies are 9.02, 9.87, and 7.13 eV, respectively, in the chosen bulk metal reference state. From Fig. 1(e), we can see that upon removal of a La or Sr atom, a big cavity is formed, which might be occupied by an oxygen atom; namely, O substituting for La point defect, O_{La} or La_v+O_i, is formed. The relaxed structure for

TABLE I. Formation energies (eV) of the various point defects. Di-oxygen molecule and La/Sr bulk metal have been chosen as reference states.

Defects	$O_{v2.08}$	$O_{v4.16}'$	$O_{v4.16}^{\cdot\cdot}$	$O_{i2.08}$	$O_{i4.16}$	$La_{v6.25}$	$La_{v12.5}$	$Sr_{v12.5}$	$O_{La6.25}$	$O_{La12.5}$
E_F	6.03	5.81	5.86	1.36	1.14	9.02	9.87	7.13	14.35	11.77

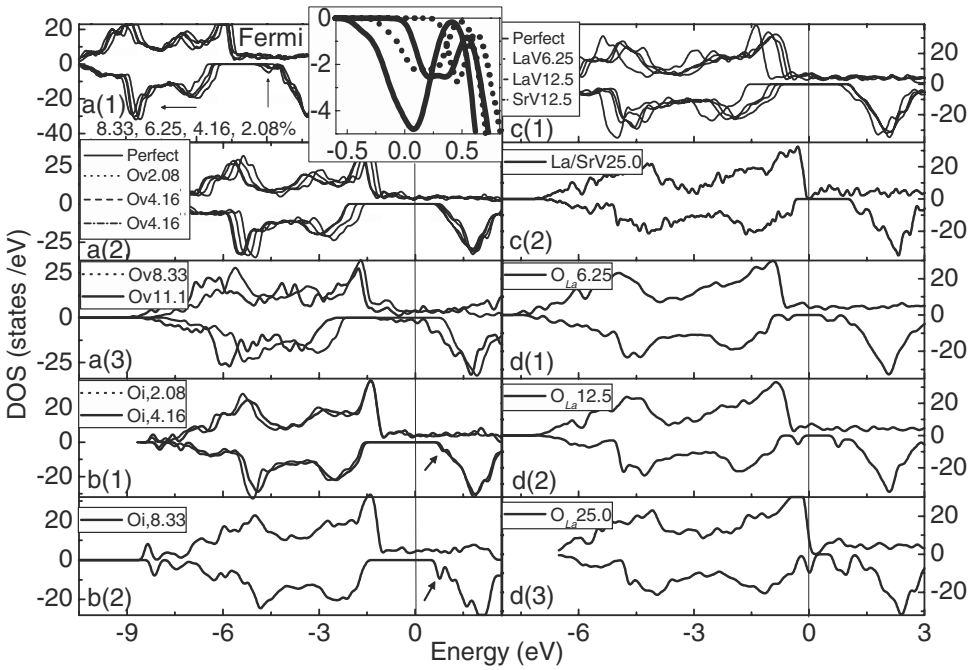

FIG. 2. [(a)(1)] The total density of states (TDOS) of unrelaxed O vacancies with concentrations of 2.08%, 4.16%, 6.25%, and 8.33% is shown from right to left (the inset shows the enlarged TDOS near the E_F), and, the comparison of the TDOS between the perfect and the relaxed oxygen vacancies [(a)(2)] $O_{v2.08}$, $O'_{v4.16}$, and $O''_{v4.16}$, [(a)(3)] $O_{v8.33}$ and $O_{v11.1}$, [(b)(1) and (b)(2)] $O_{i2.08}$, $O_{i4.16}$, and $O_{i8.33}$, [(c)(1) and [(c)(1) and (c)(2)] $La_{v6.25}$, $La_{v12.5}$, $Sr_{v12.5}$, and $La/Sr_{v25.0}$, and [(d)(1)–(d)(3)] $O_{La6.25}$, $O_{La12.5}$, and $O_{La25.0}$.

O_{La}, as shown in Fig. 1(f), has no significant difference except for the vicinal 12 O atoms that move outward and has more displacements than the La/Sr vacancy configuration due to the extra repulsive force of the O_i on other O atoms.

In order to clarify the importance of structure optimization for the electromagnetic properties of LSMO, we firstly calculated a series of O vacancy configurations in which all the degrees of freedom, but the MnO_5 units adjacent to the vacancy (unrelaxed O_v), are relaxed. The total density of states (TDOS) of unrelaxed O vacancies with concentrations of 2.08%, 4.16%, 6.25%, and 8.33% is shown from right to left in Fig. 2(a)(1), and the inset shows the enlarged TDOS near the E_F. We note that the defect states induced by Mn atoms adjacent to the unrelaxed O vacancies destroy the 100% spin polarization. However, from the latter discussion, we know that the full structure relaxations eliminate the induced defect states. In Fig. 2, we also show the comparison of the TDOS between the perfect and the relaxed oxygen vacancies $O_{v2.08}$, $O'_{v4.16}$, and $O''_{v4.16}$ [(a)(2)], $O_{v8.33}$ and $O_{v11.1}$ [(a)(3)], $O_{i2.08}$, $O_{i4.16}$, and $O_{i8.33}$ [(b)(1) and (b)(2)], $La_{v6.25}$, $La_{v12.5}$, $Sr_{v12.5}$, and $La/Sr_{v25.0}$ [(c)(1) and (c)(2)], and $O_{La6.25}$, $O_{La12.5}$, and $O_{La25.0}$ [(d)(1)–(3)]. From Fig. 2(a)(2), we note that the defect states at the E_F, shown in Fig. 2(a)(1), are completely removed by fully structure optimization. Besides, the total densities of states are rigid, which shifted toward higher binding energies by about 0.24 eV ($O_{v2.08}$), 0.48 eV ($O'_{v4.16}$ and $O''_{v4.16}$), and 0.65 eV ($O_{v8.33}$) below the E_F, indicating that the Mn d-O p hybridization is enhanced by oxygen vacancies. The Mn minority states in the conduction band also shift downward by about 0.07 eV ($O_{v2.08}$) and 0.15 eV ($O'_{v4.16}$ and $O''_{v4.16}$), and as a result, the half-metallic gaps (HMGs) are decreased to 0.449 eV ($O_{v2.08}$), 0.402 eV ($O'_{v4.16}$), and 0.358 eV ($O''_{v4.16}$) by O vacancies. Namely, in our cases (0.36 Sr doping), the oxygen vacancies with concentrations of less than 8.33% decreased the HMG by about 0.086 eV ($O_{v2.08}$), 0.133 eV ($O'_{v4.16}$), and 0.177 eV ($O''_{v4.16}$), respectively, which is not sufficient to break the 100% half-metallic characters. We know that the HMG of LSMO could be increased by higher Sr-doping concentration within the doping range of $0.25<x<0.5$, overestimation of the lattice constants by GGA and the smaller Jahn-Teller distortion. For example, for the experimental lattice parameter (a_{expt} =3.89 Å) and the theoretical equilibrium lattice parameter (a_{eq}=3.91 Å), the calculated HMGs are 0.356 and 0.535 eV for 0.36 Sr doping (in our cases) and 0.187 and 0.453 eV for 1/3 Sr doping of LSMO. Therefore, for 1/3 Sr doping of LSMO, the half-metallic characters could be almost broken by 4.16% O vacancy (HMG=0.187−0.177=0.01 eV). To our surprise, the HMG is not decreased by 8.33% O vacancy ($O_{v8.33}$), as shown in Fig. 2(a)(3), and contrarily slightly increased by about 0.03 eV. As expected, when the oxygen vacancy concentration raises to 11.1%, as shown in Fig. 2(a)(3), the half-metallic character is destroyed by induced defect states which can also be induced by an unrelaxed local O vacancy structure whatever the O vacancy concentration is [Fig. 2(a)(1)]. In addition, the e_g orbital ordering could be changed by O vacancies. Figure 3 shows the highest occupied molecular orbital (HOMO) of perfect LSMO [Fig. 3(a)], $O_{v2.08}$ [Fig. 3(b)], and the charge density distribution for the energy window of 0.8 eV width below the E_F of $O_{v11.1}$ [Fig. 3(c)]. We note that the HOMOs adjacent to the O vacancy are changed to $d_{x^2-y^2}$ [Fig. 3(b)] from d_{z^2} [Fig. 3(a)]. From Fig. 3(c), we can see that the two Mn-d_{z^2} states neighboring the vacancy are occupied by spin-down electrons, which dra-

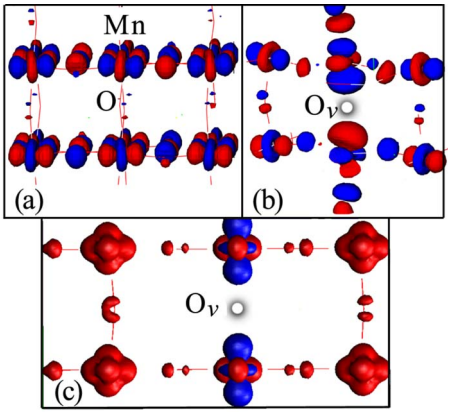

FIG. 3. (Color online) The highest occupied molecular orbital (HOMO) of (a) perfect LSMO and (b) $O_{v2.08}$, and the charge density distribution for the energy window of 0.8 eV width below the E_F of $O_{v11.1}$; the different spin components (up and down) are labeled as arrows (c).

matically deteriorate the spin current at the E_F.

Figure 4 shows the changes of the magnetic moments ($\Delta\mu_B$) [(a) and (c)] and Mulliken effective charges ($\Delta|e|$) [(b) and (d)] of all atoms in the supercell by various point defects. La/Sr, Mn, and O atoms containing in the supercell are labeled as 1–16, 17–32, and 33–81, respectively. The total magnetic moment per cell is increased by $2\mu_B$ for isolated O vacancies $O_{v2.08}$, $O'_{v4.16}$, and $O''_{v4.16}$, $4\mu_B$ for double O vacancies $O_{v8.33}$, and $0.885\mu_B$ for $O_{v11.1}$. The nearest to the vacancy the atoms are, the more the magnetic moment of atoms increases. As can be seen from Fig. 4(a), for the different oxygen vacancy configurations, the magnetic moments are maximum increased by about 0.266 ($O_{v2.08}$), 0.305 ($O'_{v4.16}$), $0.326\mu_B$ ($O''_{v4.16}$), $0.544\mu_B$ ($O_{v8.33}$), and $0.305\mu_B$ ($O_{v11.1}$) for Mn and 0.041 ($O_{v2.08}$), 0.048 ($O'_{v4.16}$), $0.042\mu_B$ ($O''_{v4.16}$), $0.088\mu_B$ ($O_{v8.33}$), and $0.082\mu_B$ ($O_{v11.1}$) for O, indicating that when the oxygen vacancy concentration increases, the magnetic moments of Mn atoms increase. However, the change

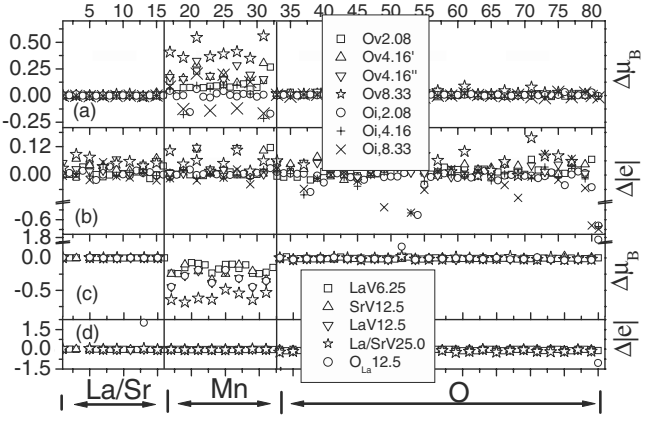

FIG. 4. [(a) and (c)] Changes of the magnetic moments ($\Delta\mu_B$) and [(b) and (d)] Mulliken effective charges ($\Delta|e|$) of all atoms in the supercell by various point defects. La/Sr, Mn, and O atoms containing in the supercell are labeled as 1-16, 17-32, and 33-81, respectively.

of moments for O and La/Sr can be neglected. From the Mulliken population analysis, as shown in Fig. 4(b), we know that the removal of the neutral oxygen atom causes a redistribution of electronic charge so that the neighboring two Mn atoms gain about 0.226 $|e|$ occupying the e_g orbital and increasing the magnetic moments; the nearest eight O atoms gain 0.42 $|e|$ and the neighboring four La/Sr gain 0.152 $|e|$, indicating that 68% of the −1.165 (corresponding to the valence of O atoms in LSMO) are attracted by the neighboring atoms and the other 32% spread over the system. However, when the concentration raises to 11.1%, the electrons gained by Mn occupy the e_g minority states and induce a defect states in E_F, which destroy the 100% half-metallic character.

For isolated interstitial oxygen, the unoccupied defect states, as indicated by the dotted arrow in Figs. 2(b)(1) and 2(b)(2), are located around 0.982 ($O_{i2.08}$), 0.864 ($O_{i4.16}$), and 0.759 eV ($O_{i8.33}$) above E_F, which are primarily composed of the antibonding σ^* molecular orbitals formed by the sp^2-hybridization states of the O_h and the O_i atoms. In addition, the occupied states located below −7 eV are primarily induced by the occupied bonding σ orbitals of the O_h and O_i atoms. Despite the resulting theoretical HMG decreases from 0.535 eV (perfect LSMO) to about 0.481 ($O_{i2.08}$), 0.444 ($O_{i4.16}$) and 0.329 eV ($O_{i8.33}$), interstitial oxygen defects make no contribution to the spin deterioration at the E_F of LSMO. From the Mulliken population analysis, as shown in Fig. 4(b), we can see that, for $O_{i2.08}$ and $O_{i4.16}$ [as indicated by open circles and crosses (+), respectively], the effective charges of O_i (corresponding to No. 81 atom) and O_h (No. 54 atom) are −0.662 $|e|$ and −0.564 $|e|$, respectively, whereas they are −1.17 $|e|$ in perfect LSMO, indicating that the O_i attracts 0.553 $|e|$ from the O_h atom and 0.109 $|e|$ from the neighboring other O atoms to compensate for its electron-deficient character. Two Mn atoms (Nos. 20 and 32) adjacent to the O_h and O_i lose 0.023 and 0.029 $|e|$ and decrease the magnetic moments by about 0.155 and $0.171\mu_B$. The effect on magnetic moments for La/Sr, O can be neglected. For $O_{i8.33}$, the effective charges of O_{h1}, O_{i1}, O_{h2}, and O_{i2} are −0.659, −0.474, −0.696, and −0.528 $|e|$, respectively, and the magnetic moments of the four Mn atoms are decreased by about 0.126, 0.141, 0.120, and 0.166, respectively.

For isolated La/Sr vacancies $La_{v6.25}$, $La_{v12.5}$, and $Sr_{v12.5}$, the calculated formation energies are 9.02, 9.87, and 7.13 eV, respectively. As can be seen from Fig. 2(c)(1), the total densities of states are shifted upward by about 0.40 eV ($La_{v6.25}$), 0.60 eV ($La_{v12.5}$), and 0.50 eV ($Sr_{v12.5}$), below the E_F, indicating that the Mn d-O p hybridization is attenuated by La/Sr vacancies. However, the Mn minority state in the conduction band shifts upward by about 0.285 eV for all the isolated La/Sr vacancies. When the La/Sr vacancy concentration increases up to 25.0%, as shown in Fig. 2(c)(2), the T_{2g} states are shifted upward by about 0.95 eV and the majority spin at the Fermi level is decreased dramatically.

The total magnetic moment per unit defect cell is decreased by $3\mu_B$, $3\mu_B$, and $5\mu_B$ for isolated La/Sr vacancy $La_{v6.25}$, $La_{v12.5}$, and $Sr_{v12.5}$ and $2\mu_B$ for double La/Sr vacancies $La/Sr_{v25.0}$. From Fig. 4(c), we can see that the higher the concentration of La/Sr vacancies, the smaller the magnetic

moments of Mn atoms are. For the different La/Sr vacancy configurations, the magnetic moments are maximum decreased by about 0.241 ($La_{v6.25}$), 0.451 ($La_{v12.5}$), 0.336μ_B ($Sr_{v12.5}$), and 0.682μ_B ($La/Sr_{v25.0}$) for Mn. The change for O and La/Sr can be neglected. From the Mulliken population analysis, as shown in Fig. 4(d), we know that the effect on charge for all atoms can be neglected.

For isolated O substituting for La, $O_{La6.25}$, and $O_{La12.5}$, the calculated formation energies are 14.35 and 11.77 eV, respectively. As can be seen from Fig. 2(d)(1) and 2(d)(2), the total densities of states are shifted upward by about 0.398 eV ($O_{La6.25}$) and 0.593 eV ($O_{La12.5}$) below E_F. Compared to other point defects, Mn-T_{2g} states are greatly broadened by O_{La} defects, and the total densities of states character are somewhat similar to La/Sr vacancies. The differences are the two induced defect states located at both sides of E_F. With increasing concentration, the two defect states move toward E_F and come close to one another. The half-metallic character has been broken by defect states emerged from the minority valence band in the case of $O_{La12.5}$. When the O_{La} concentration raises to 25.0%, as shown in Fig. 2(d)(3), a strong peak near E_F mainly for the majority spin but with some weight on the minority spin is induced, which breaks the half metallicity of the system due to the changes in the electronic occupation for the e_g states.

In summary, first-principles total-energy electronic structure calculations for various point defects with different concentrations in LSMO have been carried out. Oxygen vacancies with concentrations of less than 8.33% decrease the HMG but are not sufficient to break the half-metallic characters. When the oxygen vacancy concentration raises to 11.1%, the half-metallic character is destroyed by induced defect states. O substituting for La with a concentration of 12.5% is also responsible for the spin deterioration of the LSMO. Interstitial oxygen defects with concentrations of 2.08%–8.33% make no contribution to the spin deterioration of LSMO.

Kunpeng Wang thanks the Alexander von Humboldt Foundation for all supports during his study in Germany.

*klaus.betzler@uos.de

[1] K. Dörr, J. Phys. D **39**, R125 (2006); M. B. Salamon and M. Jaime, Rev. Mod. Phys. **73**, 583 (2001); J. M. D. Coey, M. Viret, and S. Von Molnar, Adv. Phys. **48**, 167 (1999); C. N. R. Rao, A. K. Cheetham, and R. Mahesh, Chem. Mater. **8**, 2421 (1996).

[2] I. Žutić, J. Fabian, and S. Das Sarma, Rev. Mod. Phys. **76**, 323 (2004); S. Ganichev and W. Prettl, J. Phys.: Condens. Matter **15**, R935 (2003); S. A. Wolf, D. D. Awschalom, R. A. Buhrman, J. M. Daughton, S. von Molnár, M. L. Roukes, A. Y. Chtchelkanova, and D. M. Treger, Science **294**, 1488 (2001).

[3] J.-H. Park, E. Vescovo, H.-J. Kim, C. Kwon, R. Ramesh, and T. Venkatesan, Nature (London) **392**, 794 (1998).

[4] M. Bowen, M. Bibes, A. Barthélémy, J.-P. Contour, A. Anane, Y. Lemaître, and A. Fert, Appl. Phys. Lett. **82**, 233 (2003).

[5] M. Viret, M. Drouet, J. Nassar, J. P. Contour, C. Fermon, and A. Fert, Europhys. Lett. **39**, 545 (1997).

[6] M. Johnson, J. Supercond. **14**, 273 (2001).

[7] E. I. Rashba, Phys. Rev. B **62**, R16267 (2000).

[8] L. E. Hueso, J. M. Pruneda, V. Ferrari, G. Burnell, J. P. Valdé-Herrera, B.-J. D. Simons, P. B. Littlewood, E. Artacho, A. Fert, and N. D. Mathur, Nature (London) **445**, 410 (2007).

[9] H. Yamada, Y. Ogawa, Y. Ishii, H. Sato, M. Kawasaki, H. Akoh, and Y. Tokura, Science **305**, 646 (2004).

[10] R. Bertacco, M. Riva, M. Cantoni, L. Signorini, and F. Ciccacci, Appl. Phys. Lett. **86**, 252502 (2005).

[11] S. Picozzi, C. Ma, Z. Yang, R. Bertacco, M. Cantoni, A. Cattoni, D. Petti, S. Brivio, and F. Ciccacci, Phys. Rev. B **75**, 094418 (2007).

[12] J. M. Soler, E. Artacho, J. D. Gale, A. García, J. Junquera, P. Ordejón, and D. Sánchez-Portal, J. Phys.: Condens. Matter **14**, 2745 (2002).

[13] J. P. Perdew, K. Burke, and M. Ernzerhof, Phys. Rev. Lett. **77**, 3865 (1996).

[14] E. Artacho, D. Sánchez-Portal, P. Ordejón, A. García, and J. M. Soler, Phys. Status Solidi B **215**, 809 (1999).

[15] V. I. Anisimov, J. Zaanen, and O. K. Andersen, Phys. Rev. B **44**, 943 (1991).

[16] V. Ferrari, J. M. A. Pruneda, and E. Artacho, Phys. Status Solidi A **203**, 1437 (2006).

[17] J. M. Pruneda, V. Ferrari, P. B. Littlewood, N. A. Spaldin, and E. Artacho, arXiv:0705.0335 (unpublished).

[18] R. Vidya, P. Ravindran, P. Vajeeston, A. Kjekshus, and H. Fjellvág, Phys. Rev. B **69**, 092405 (2004).

[19] C. O. Paiva-Santos, R. F. C. Marques, M. Jafelicci, Jr., and L. C. Varanda, Powder Diffr. **17**, 149 (2002).

[20] J. P. Crocombette, F. Jollet, T. N. Le, and T. Petit, Phys. Rev. B **64**, 104107 (2001).

[21] J. D. Cox, Pure Appl. Chem. **54**, 1239 (1982).

[22] K. P. Wang, C. S. Fang, J. X. Zhang, C. S. Liu, R. I. Boughton, S. L. Wang, and X. Zhao, Phys. Rev. B **72**, 184105 (2005).

[23] Y. G. Jin and K. J. Chang, Phys. Rev. Lett. **86**, 1793 (2001).